Liquid Crystals
Publication details, including instructions for authors and subscription information:
http://www.informaworld.com/smpp/title~content=t713926090

Synthesis and characterization of non-symmetric chiral dimers

C. V. Yelamaggad[a]; G. Shanker[a]
[a] Centre for Liquid Crystal Research, Jalahalli, Bangalore 560 013, India

To cite this Article Yelamaggad, C. V. and Shanker, G.(2007) 'Synthesis and characterization of non-symmetric chiral dimers', Liquid Crystals, 34: 9, 1045 — 1057
To link to this Article: DOI: 10.1080/02678290701616280
URL: http://dx.doi.org/10.1080/02678290701616280

Liquid Crystfals, Vol. 34, No. 9, September 2007, 1045–1057

Taylor & Francis
Taylor & Francis Group

Synthesis and characterization of non-symmetric chiral dimers

C. V. YELAMAGGAD* and G. SHANKER
Centre for Liquid Crystal Research, Jalahalli, Bangalore 560 013, India

(*Received 30 May 2007; accepted in revised form 7 August 2007*)

A new class of cholesterol-based non-symmetric dimers have been synthesized and characterized. They comprise *O*-alkylated cinnamic acid and pro-mesogenic cholesterol segments interlinked covalently through a methylene spacer varying in its length and parity. All the dimers and some of the key precursors have been studied for their phase behaviour. All the intermediates show mesomorphism. Importantly, the thermal properties of dimers are found to be critically dependent on the parity of the flexible spacer. The dimers with odd-parity spacer display chiral nematic and/or twist grain boundary phases. In contrast, the dimers with even-parity spacer are either crystalline or exhibit metastable chiral nematic and/or twist grain boundary phases with the exception of one compound for which two unknown mesophases have been observed. The odd–even effect was found to be indistinct for selective reflection wavelengths of the chiral nematic phase. For some dimers, a variation in the pitch of the chiral nematic phase as a function of temperature was observed. Cyclic voltammetry experiments revealed the electrochemical properties of a representative liquid crystal dimer.

1. Introduction

Liquid crystal (LC) phases are ordered fluids featuring unique optical, electrical, magnetic and mechanical properties [1]. Consequently, thermotropic LC phases formed of conventional rod-like or disc-shaped anisotropic molecules have been used in many practical technological applications, such as display devices [2]. However, over the years it has been shown that LC behaviour with improved characteristics is achievable with molecules differing in their shape anisotropy compared with conventional LCs [3]. Of several kinds of such non-conventional molecular architectures known, the LC dimers [4–13] composed of either identical (symmetrical) or non-identical (non-symmetrical) mesogenic segments connected through a flexible central spacer are not only exciting objects of synthesis but are also gaining immense importance from both fundamental [4] and application viewpoints [5]. One of the fascinating characteristics of LC dimers is the critical dependence of their thermal properties on the parity (i.e. odd or even), and the chemical nature of linking groups between the spacer and the anisometric segments. This is especially true in the case of non-symmetrical dimers, since they exhibit rich mesomorphism [4a].

Many studies of non-symmetrical dimers have been reported [6–13]. Among these, a series of compounds, in which 4-methoxy-substituted cinnamic acid and cyanobiphenyl entities interlinked through a flexible spacer, are quite distinct [7]. For instance, the use of a cinnamic acid core as the mesogenic segment, which is almost half the length of other rod-like cores, makes them a special kind of dimer. Additionally, the dimers composed of an odd number of methylene units in the spacer attain a rod-like shape, instead of the usual bent shape. This is because, in the all-*trans* conformation, the cinnamoate moiety lies nearly parallel to the cyanobiphenyl core. Thus, while determining the parity of the spacer, –CO.O– and –O– linking groups have been included. Furthermore, several of these compounds exhibit nematic behaviour. On the other hand, non-symmetric dimers [9–13] formed by combining a cholesteryl ester moiety and aromatic mesogens, such as Schiff's base, azo, stilbene, ester, tolane, salicylaldimine, biphenyl, etc, through a polymethylene spacer have continued to attract the attention of researchers since their invention [9a]. This can be ascribed to their unique molecular structural features, which have resulted not only in stabilized, technologically important mesophases over wide thermal range [11] but also in polymesomorphic sequences of considerable fundamental research interest [9–12]. In particular, their phase behaviour seems to be critically dependant on the nature of the flexible spacer and non-cholesteryl (aromatic) mesogenic unit [9–13]. Consequently, they offer new synthetic concepts and targets to chemists. In order to further our understanding of the structure–property correlation, and

*Corresponding author. Email: Yelamaggad@gmail.com

Liquid Crystfals
ISSN 0267-8292 print/ISSN 1366-5855 online
http://www.tandf.co.uk/journals
DOI: 10.1080/02678290701616280

especially to examine the effect of cinnamic acid core on the thermal behaviour of cholesterol-based dimers, the present study was undertaken. Here we report the synthesis and characterization of new dimers, the cholsteryloxyalkyl ω-(4-(alkoxy)phenyl)acrylates; the molecular structures of which are shown in scheme 1. The acronym employed to refer to the these dimers is **ChO*n*CO*m*** where **Ch** and **C** refer to cholesteryl and cinnamoate segments, respectively, and ***n*** and ***m*** denote the number of methylene units in the flexible spacer and the length of the alkoxy chain, respectively.

2. Experimental

2.1. *General*

Chemicals were purchased from either Aldrich or Lancaster or local companies, and were used without further purification. All the solvents were purified and dried by known methods prior to use. The intermediates and target compounds were purified by column chromatographic technique using either silica gel (400 mesh) or neutral aluminium oxide as a stationary phase. Thin layer chromatography (TLC) was performed on aluminium sheets pre-coated with silica gel (Merck, Kieselgel 60, F_{254}). UV–visible spectra were recorded using a Perkin Elmer Lambda 20 UV–Vis spectrometer. FTIR spectra were recorded on a Perkin Elmer Spectrum 1000 FTIR spectrophotometer using KBr disks. ^{1}H and ^{13}C NMR spectra were recorded on a Bruker AMX-400 (400 MHz) or a Bruker Aveance series DPX-200 (200 MHz) spectrometer in $CDCl_3$ with $SiMe_4$ (TMS) as an internal standard. The chemical shifts are reported in parts per million (ppm) relative to TMS. Mass spectra were recorded on a Jeol-JMS-600H spectrometer in FAB^+ mode using 3-nitrobenzyl alcohol as a liquid matrix. Elemental analyses were carried out using Eurovector model EA 3000 CHNS analyser. Circular dichroism (CD) measurements were recorded with the aid of Jasco J-810 spectropolorimeter. The identification of the mesophases and the transition temperatures of the compounds were determined using a polarizing optical microscope (POM, Leitz DMRXP) in conjunction with a programmable hot stage (Mettler FP90). The transition temperatures and associated enthalpies were determined by differential scanning calorimetry (DSC, Perkin Elmer DSC7). Cyclic voltammetry measurements were carried out with CH instrument (Texas, USA) model 619B series computer-controlled potentiostat.

2.2. *Synthesis and molecular characterization*

Dimers with a 4-*n*-alkoxy-substituted cinnamoate segment covalently tethered via either penta-, hexa-, hepta- or octamethylene spacer to the cholesteryl entity were prepared following the synthetic route shown in scheme 1. Cholesteryloxyalkanols (**1a**–**1d**) [13, 14] were obtained by reacting α,ω-alkanediols with cholesteryl 4-methylphenylsulfonate (**3**) in dry 1,4-dioxane refluxed under inert atmosphere. The latter compound **3** was synthesized according to the procedure reported elsewhere [15] with some modification (see experimental section for details). The other key intermediates, the 4-*n*-alkoxycinnamic acids **2a**–**2d**, were prepared in two steps. 4-Hydroxybenzaldehyde was *O*-alkylated with either *n*-bromoalkanes in presence of a mild base to obtain aldehydes **4a**–**4d**. Knoevenagel condensation of malonic acid and aldehydes **4a**–**4d** furnished the acids **2a**–**2d**. Finally, the condensation of alcohols **1a**–**1d** with acids **2a**–**2d** using dicyclohexylcarbodimide (DCC) and 4-(*N*,*N*-dimethylamino)pyridine (DMAP) in dichloromethane yielded the required dimers in excellent yields. The molecular structures of all the intermediates and target compounds were evidenced by spectroscopic (FTIR, NMR and MS) and elemental analyses.

2.2.1. General procedure for the preparation of 4-n-alkoxycinnamic acids. To prepare 4-*n*-alkoxycinnamic acids (**2a**–**2d**) [16], 4-*n*-alkoxybenzaldehydes (7.63 mmol, 1 equiv.), malonic acid (11.43 mmol, 1.5 equiv.), pyridine and a catalytic amount of piperidine were refluxed for 10 h at 120°C. The reaction mixture was poured into ice-cold 2N HCl until all the pyridine was neutralized to yield a white solid. The crude mass was extracted with EtOAc, washed with water, brine, dried over anhydrous Na_2SO_4 and concentrated. The product was further purified by recrystallization using EtOAc:EtOH (1:10) to yield a pure white solid.

2.2.2. 4-*n*-Dodecyloxycinnamic acid (2a). R_f=0.32 in 30% CH_2Cl_2–hexanes; yield: 82%. Phase sequences (temperatures in °C [enthalpies in J g^{-1}]): crystal (Cr) 128.3 [56.9] smectic C (SmC) 157.1 [7.7] nematic (N) 160.4 [6.4] isotropic (I); I 157.8 [4.5] N 155 [5.3] SmC 124 [52.2] Cr. IR (neat): ν_{max} in cm^{-1} 2921, 2850, 1674, 1603, 1173. ^{1}H NMR (200 MHz, $CDCl_3$): δ 7.81 (d, 1H, J=15.8 Hz 1 × olefinic), 7.55 (d, J=8.6 Hz, 2H, Ar), 6.97 (d, J=8.6 Hz. 2H, Ar), 6.39 (d, 1H, J=16.0 Hz 1 × olefinic), 4.07 (t, J=6.4 Hz, 2H, 1 × OCH_2), 1.87–1.31 (m, 20H, 10 × CH_2), 0.96 (t, J=6.6 Hz, 3H, 1 × CH_3). MS (FAB+): m/z calculated for $C_{21}H_{33}O_3$ (M+1), 333.24; found, 333.40. Elemental analysis: calculated for $C_{21}H_{32}O_3$, C 75.86, H 9.70; found, C 75.94, H 9.97%.

2.2.3. 4-*n*-Hexadecyloxycinnamic acid (2b). R_f=0.34 in 30% CH_2Cl_2–hexanes; yield: 80%. Phase sequence: Cr

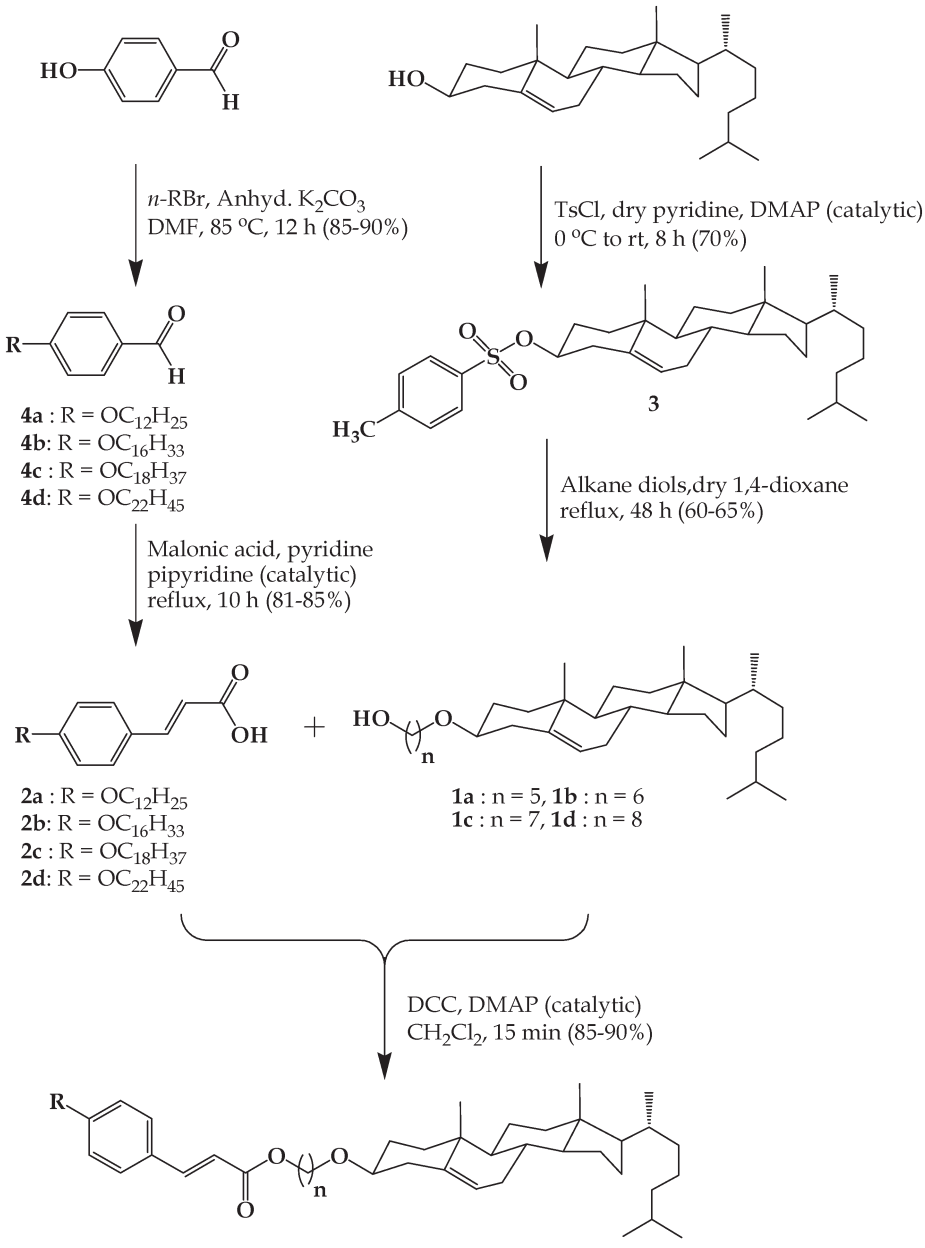

ChO5CO12: n = 5; R = $OC_{12}H_{25}$ **ChO5CO16**: n = 5; R = $OC_{16}H_{33}$
ChO6CO12: n = 6; R = $OC_{12}H_{25}$ **ChO6CO16**: n = 6; R = $OC_{16}H_{33}$
ChO7CO12: n = 7; R = $OC_{12}H_{25}$ **ChO7CO16**: n = 7; R = $OC_{16}H_{33}$
ChO8CO12: n = 8; R = $OC_{12}H_{25}$ **ChO8CO16**: n = 8; R = $OC_{16}H_{33}$

ChO5CO18: n = 5; R = $OC_{18}H_{37}$ **ChO5CO22**: n = 5; R = $OC_{22}H_{45}$
ChO6CO18: n = 6; R = $OC_{18}H_{37}$ **ChO6CO22**: n = 6; R = $OC_{22}H_{45}$
ChO7CO18: n = 7; R = $OC_{18}H_{37}$ **ChO7CO22**: n = 7; R = $OC_{22}H_{45}$
ChO8CO18: n = 8; R = $OC_{18}H_{37}$ **ChO8CO22**: n = 8; R = $OC_{22}H_{45}$

Scheme 1. Synthesis of cholsteryloxyalkyl ω-(4-(alkoxy)phenyl)acrylates, **ChO*n*CO*m***.

123.5 [35.3] SmC 152.6 [6.2] I; I 146 [5.3] SmC 120.9 [39.6] Cr. IR (neat): ν_{max} in cm^{-1} 2921, 2850, 1674, 1603, 1173. ^1H NMR (200 MHz, $CDCl_3$): δ 7.77 (d, 1H, J=16.0 Hz, 1 × olefinic), 7.51 (d, J=8.0 Hz, 2H, Ar), 6.92 (d, J=8.0 Hz. 2H, Ar), 6.35 (d, 1H, J=16.0 Hz, 1 × olefinic), 4.02 (t, J=6.0 Hz, 2H, 1 × OCH_2), 1.83–1.26 (m, 28H, 14 × CH_2), 0.91 (t, J=6.0 Hz, 3H, 1 × CH_3). MS (FAB+): m/z calculated for $C_{25}H_{41}O_3$ (M+1), 389.30; found, 389.50. Elemental analysis: calculated for $C_{25}H_{40}O_3$, C 77.27, H 10.38; found, C 77.54, H 10.21%.

2.2.4. 4-*n*-Octadecyloxycinnamic acid (2c). R_f=0.36 in 30% CH_2Cl_2–hexanes; yield: 83%. Phase sequence: Cr 120.8 [69.6] SmC 154.1 [18.0] I; I 151.7 [17.5] SmC 117.4 [70.0] Cr. IR (neat): ν_{max} in cm^{-1} 2919, 2850, 1676, 1604, 1172. ^1H NMR (400 MHz, $CDCl_3$): δ 7.77 (d, 1H, J=15.9 Hz, 1 × olefinic), 7.51 (d, J=8.0 Hz, 2H, Ar), 6.92 (d, J=8.0 Hz. 2H, Ar), 6.35 (d, 1H, J=16.0 Hz, 1 × olefinic), 4.01 (t, J=5.6 Hz, 2H, 1 × OCH_2), 1.85–1.30 (m, 32H, 16 × CH_2), 0.95 (t, J=6.0 Hz, 3H, 1 × CH_3). MS (FAB+): m/z calculated for $C_{27}H_{45}O_3Na$, (M+1) 440.30; found, 440.30. Elemental analysis: calculated for $C_{27}H_{44}O_3$, C 77.74, H 10.79; found, C 77.83, H 10.64%.

2.2.5. 4-*n*-Docosyloxy-cinnamic acid (2d). R_f=0.40 in 30% CH_2Cl_2–hexanes; yield: 75%. IR (neat): ν_{max} in cm^{-1} 2918, 2849, 1681, 1604, 1173. ^1H NMR (400 MHz, C_6D_6+CD_3OD): δ 7.78 (d, 1H, J=15.9 Hz, 1 × olefinic), 7.15 (d, J=8.7 Hz, 2H, Ar), 6.68 (d, J=8.7 Hz, 2H, Ar), 6.39 (d, 1H, J=15.9 Hz, 1 × olefinic), 3.7 (t, J=6.4 Hz, 2H, 1 × OCH_2), 1.65–1.25 (m, 40H, 20 × CH_2), 0.85 (t, J=6.4 Hz, 3H, 1 × CH_3). MS (FAB+): m/z calculated for $C_{31}H_{52}O_3$, 472.39; found, 472.91. Elemental analysis: calculated for $C_{31}H_{52}O_3$, C 78.76, H 11.09; found, C 78.83, H 11.45%.

2.2.6. Cholsteryloxyalkyl 3-(4-(*n*-alkoxy)phenyl) acrylate (ChO*n*CO*m*). To a stirring solution of cholesteryloxy ω-hydroxyalkanes (**1a**–**1d**) (0.42 mmol, 1 equiv.), 4-*n*-alkoxycinnamic acid (**2b**–**2c**) (0.42 mmol, 1 equiv.) and DMAP (0.02 mmol, 0.05 equiv.) in anhydrous CH_2Cl_2 (20 ml) was added a solution of DCC (0.63 mmol, 1.5 equiv.) in CH_2Cl_2 (20 mL) added at room temperature and the mixture was stirred for 4 h. The precipitated *N*,*N*′-dicyclohexylurea was filtered off; the filtrate was diluted with CH_2Cl_2 (20 ml) and washed with 0.5N HCl, saturated Na_2CO_3 solution, water and dried over anhydrous Na_2SO4. Evaporation of solvent in vacuo furnished the crude product that was purified by column chromatography on neutral alumina using 10% ethyl acetate–hexanes as eluent. The product was recrystallized repeatedly from the solvent mixture CH_2Cl_2–ethanol (1:10) to obtain a white solid.

2.2.7. Cholsteryloxypentyl 3-(4-(*n*-dodecyloxy)phenyl)-acrylate (ChO5CO12). R_f=0.76 in 20% EtOAc–hexanes; yield: 64%. IR (KBr pellet): ν_{max} in cm^{-1} 2926, 2854, 1713, 1603, 1251, 1164. UV–visible: λ_{max}=310.1 nm, $\in = 2.66 \times 10^4$ L mol^{-1} cm^{-1}. ^1H NMR (400 MHz, $CDCl_3$): δ 7.64 (d, J=16 Hz, 1H, 1 × olefinic), 7.47 (d, J=8.7 Hz, 2H, Ar), 6.9 (d, J=8.6 Hz, 2H, Ar), 6.31 (d, J=16 Hz, 1H, 1 × olefinic), 5.34 (brd, J=5 Hz, 1H, 1 × olefinic), 4.18 (t, 2H, J=6.6 Hz, 1 × OCH_2), 3.99 (t, 2H, J=6.5 Hz, 1 × OCH_2), 3.47 (t, 2H, J=6.6 Hz, 1 × OCH_2), 3.13 (m, 1H, 1 × CH-O), 2.4–0.67 (m, 72H, 6 × CH, 24 × CH_2, 6 × CH_3)/MS (FAB^+): m/z calculated for $C_{53}H_{87}O_4$ (M+1), 787.65; found, 787.95. Elemental analysis: calculated for $C_{53}H_{86}O_4$, C 80.86, H 11.01; found, C 80.98, H 11.01%.

2.2.8. Cholsteryloxyhexyl 3-(4-(*n*-dodecyloxy)phenyl)-acrylate (ChO6CO12). R_f=0.84 in 20% EtOAc–hexanes; yield: 63%. IR (KBr pellet): ν_{max} in cm^{-1} 2925, 2848, 1706, 1629, 1254, 1165. UV–visible: λ_{max}=310.9 nm, $\in = 2.91 \times 10^4$ L mol^{-1} cm^{-1}. ^1H NMR (400 MHz, $CDCl_3$): δ 7.65 (d, J=16 Hz, 1H, 1 × olefinic), 7.47 (d, J=8.7 Hz, 2H, Ar), 6.9 (d, J=8.7 Hz, 2H, Ar), 6.32 (d, J=15.9 Hz, 1H, 1 × olefinic), 5.34 (brd, J=5.1 Hz, 1H, 1 × olefinic), 4.19 (t, 2H, J=6.6 Hz, 1 × OCH_2), 3.99 (t, 2H, J=6.5 Hz, 1 × OCH_2), 3.48 (t, 2H, J=6.6 Hz, 1 × OCH_2), 3.15 (m, 1H, 1 × CH–O), 2.41–0.67 (m, 74H, 6 × CH, 25 × CH_2, 6 × CH_3). MS (FAB^+): m/z calculated for $C_{54}H_{88}O_4$, 800.67; found, 800.24. Elemental analysis: calculated for $C_{54}H_{88}O_4$, C 80.94, H 11.07; found, C 81.16, H 11.37%.

2.2.9. Cholsteryloxyheptyl 3-(4-(*n*-dodecyloxy)phenyl)-acrylate (ChO7CO12). R_f=0.86 in 20% EtOAc–hexanes; yield: 69%. IR (KBr pellet): ν_{max} in cm^{-1} 2933, 2853, 1703, 1631, 1252, 1169. UV–visible: λ_{max}=310.33 nm, $\in = 3.15 \times 10^4$ L mol^{-1} cm^{-1}. ^1H NMR (400 MHz, $CDCl_3$): δ 7.65 (d, J=16.0 Hz, 1H, 1 × olefinic), 7.47 (d, J=8.7 Hz, 2H, Ar), 6.90 (d, J=8.7 Hz, 2H, Ar), 6.32 (d, J=15.9 Hz, 1H, 1 × olefinic), 5.35 (brd, J=4.8 Hz, 1H, 1 × olefinic), 4.20 (t, 2H, J=6.6 Hz, 1 × OCH_2), 3.99 (t, 2H, J=6.5 Hz, 1 × OCH_2), 3.47 (t, 2H, J=6.8 Hz, 1 × OCH_2), 3.13 (m, 1H, 1 × CH–O), 2.37–0.67 (m, 76H, 6 × CH, 26 × CH_2, 6 × CH_3). ^{13}C NMR (400 MHz, CDCl3): 167.54, 160.98, 144.37, 141.18, 129.72, 126.97, 121.45, 115.54, 114.81, 80.01, 68.17, 68.08, 64.53, 56.81, 56.17, 50.22, 42.35, 39.82, 39.55, 39.24, 37.33, 36.94,

36.22, 35.83, 31.96, 29.68, 31.92, 30.16, 29.68, 29.63, 29.61, 29.4, 29.2, 28.74, 28.52, 28.28, 28.06, 26.16, 26.04, 26.0, 24.33, 23.86, 22.88, 22.74, 22.61, 21.09, 19.43, 18.75, 14.18, 11.89. MS (FAB^+): m/z calculated for $C_{55}H_{90}O_4$, 814.68; found, 814.51. Elemental analysis: calculated for $C_{55}H_{90}O_4$, C 81.02, H 11.13; found, C 81.28, H 11.42%.

2.2.10. Cholsteryloxyoctyl 3-(4-(*n*-dodecyloxy)phenyl)-acrylate (ChO8CO12). R_f=0.89 in 20% EtOAc–hexanes; yield: 70%. IR (KBr pellet): ν_{max} in cm^{-1} 2926, 2849, 1729, 1628, 1262, 1189. UV–visible: λ_{max}=310.53 nm, $\in = 5.95 \times 10^3\,L\,mol^{-1}\,cm^{-1}$. ^1H NMR (400 MHz, $CDCl_3$): δ 7.65 (d, J=16.0 Hz, 1H, 1 × olefinic), 7.47 (d, J=8.7 Hz, 2H, Ar), 6.90 (d, J=8.7 Hz, 2H, Ar), 6.32 (d, J=15.9 Hz, 1H, 1 × olefinic), 5.35 (brd, J=5.0 Hz, 1H, 1 × olefinic), 4.19 (t, 2H, J=6.6 Hz, 1 × OCH_2), 3.99 (t, 2H, J=6.5 Hz, 1 × OCH_2), 3.46 (t, 2H, J=6.8 Hz, 1 × OCH_2), 3.13 (m, 1H, 1 × CH–O), 2.37–0.67 (m, 78H, 6 × CH, 27 × CH_2, 6 × CH_3). MS (FAB^+): m/z calculated for $C_{56}H_{92}O_4$, 828.7; found, 828.7. Elemental analysis: calculated for $C_{56}H_{92}O_4$, C 81.10, H 11.18; found, C 81.33, H 11.07%.

2.2.11. Cholsteryloxypentyl 3-(4-(*n*-hexadecyloxy)phenyl)-acrylate (ChO5CO16). R_f=0.80 in 20% EtOAc–hexanes; yield: 66%. IR (KBr pellet): ν_{max} in cm^{-1} 2925, 2852, 1709, 1602, 1251, 1167. UV–visible: λ_{max}=310.05 nm, $\in = 2.37 \times 10^4\,L\,mol^{-1}\,cm^{-1}$. ^1H NMR (400 MHz, $CDCl_3$): δ 7.64 (d, J=16.0 Hz, 1H, 1 × olefinic), 7.46 (d, J=8.6 Hz, 2H, Ar), 6.90 (d, J=8.6 Hz, 2H, Ar), 6.31 (d, J=15.9 Hz, 1H, 1 × olefinic), 5.32 (brd, J=5.0 Hz, 1H, 1 × olefinic), 4.20 (t, 2H, J=6.6 Hz, 1 × OCH_2), 3.99 (t, 2H, J=6.5 Hz, 1 × OCH_2), 3.49 (t, 2H, J=6.7 Hz, 1 × OCH_2), 3.14 (m, 1H, 1 × CH–O), 2.32–0.67 (m, 80H, 6 × CH, 28 × CH_2, 6 × CH_3). MS (FAB^+): m/z calculated for $C_{57}H_{94}O_4$, 842.72; found, 841.9. Elemental analysis: calculated for $C_{57}H_{94}O_4$, C 81.18, H 11.23; found, C 81.39, H 11.38%.

2.2.12. Cholsteryloxyhexyl 3-(4-(*n*-hexadecyloxy)phenyl)-acrylate (ChO6CO16). R_f=0.82 in 20% EtOAc–hexanes; yield: 64%. IR (KBr pellet): ν_{max} in cm^{-1} 2926, 2851, 1709, 1603, 1253, 1167. UV–visible: λ_{max}=310.5 nm, $\in = 1.76 \times 10^4\,L\,mol^{-1}\,cm^{-1}$; ^1H NMR (400 MHz, $CDCl_3$): δ 7.64 (d, J=15.9 Hz, 1H, 1 × olefinic), 7.47 (d, J=8.6 Hz, 2H, Ar), 6.89 (d, J=8.6 Hz, 2H, Ar), 6.32 (d, J=16.0 Hz, 1H, 1 × olefinic), 5.32 (brd, J=5.0 Hz, 1H, 1 × olefinic), 4.20 (t, 2H, J=6.5 Hz, 1 × OCH_2), 3.99 (t, 2H, J=6.5 Hz, 1 × OCH_2), 3.47 (t, 2H, J=6.5 Hz, 1 × OCH_2), 3.13 (m, 1H, 1 × CH–O), 2.31–0.67 (m, 82H, 6 × CH, 29 × CH_2, 6 × CH_3,). MS (FAB^+): m/z calculated for $C_{58}H_{96}O_4$, 856.73; found, 856.05. Elemental analysis: calculated for $C_{58}H_{96}O_4$, C 81.25, H 11.29; found, C 81.08, H 11.34%.

2.2.13. Cholsteryloxyheptyl 3-(4-(*n*-hexadecyloxy)phenyl)-acrylate (ChO7CO16). R_f=0.83 in 20% EtOAc–hexanes; yield: 65%. IR (KBr pellet): ν_{max} in cm^{-1} 2922, 2850, 1704, 1605, 1252, 1163. UV–visible: λ_{max}=310.02 nm, $\in = 2.30 \times 10^4\,L\,mol^{-1}\,cm^{-1}$. ^1H NMR (400 MHz, $CDCl_3$): δ 7.65 (d, J=15.9 Hz, 1H, 1 × olefinic), 7.47 (d, J=8.6 Hz, 2H, Ar), 6.89 (d, J=8.7 Hz, 2H, Ar), 6.32 (d, J=15.9 Hz, 1H, 1 × olefinic), 5.34 (brd, J=4.7 Hz, 1H, 1 × olefinic), 4.19 (t, 2H, J=6.6 Hz, 1 × OCH_2), 3.99 (t, 2H, J=6.6 Hz, 1 × OCH_2), 3.47 (t, 2H, J=6.8 Hz, 1 × OCH_2), 3.12 (m, 1H, 1 × CH–O), 2.37–0.67 (m, 84H, 6 × CH, 30 × CH_2, 6 × CH_3). ^{13}C NMR (400 MHz, $CDCl_3$): 167.53, 160.99, 144.37, 141.18, 129.73, 126.97, 121.46, 115.55, 114.81, 79.0, 68.17, 68.08, 64.53, 56.82, 56.18, 50.23, 42.35, 39.82, 39.56, 39.25, 37.33, 36.94, 36.23, 35.83, 31.98, 31.93, 30.17, 29.75, 29.64, 29.42, 29.2, 28.75, 28.53, 28.29, 28.06, 26.17, 26.05, 26.01, 24.34, 23.87, 22.88, 22.75, 22.62, 21.1, 19.43, 18.76, 14.19, 11.89. MS (FAB^+): m/z calculated for $C_{59}H_{98}O_4$: 870.75; found, 870.57. Elemental analysis: calculated for $C_{59}H_{98}O_4$, C 81.32, H 11.34; found, C 81.15, H 11.62%.

2.2.14. Cholsteryloxyoctyl 3-(4-(*n*-hexadecyloxy)phenyl)-acrylate(ChO8CO16). R_f=0.84 in 20% EtOAc–hexanes; yield: 69%. IR (KBr pellet): ν_{max} in cm^{-1} 2920, 2849, 1709, 1604, 1253, 1168. UV–visible: λ_{max}=310.30 nm, $\in = 2.41 \times 10^4\,L\,mol^{-1}\,cm^{-1}$. ^1H NMR (400 MHz, $CDCl_3$): δ 7.65 (d, J=16.0 Hz, 1H, 1 × olefinic), 7.47 (d, J=8.7 Hz, 2H, Ar), 6.90 (d, J=8.7 Hz, 2H, Ar), 6.32 (d, J=15.9 Hz, 1H, 1 × olefinic), 5.34 (brd, J=5.0 Hz, 1H, 1 × olefinic), 4.19 (t, 2H, J=6.7 Hz, 1 × OCH_2), 3.99 (t, 2H, J=6.5 Hz, 1 × OCH_2), 3.46 (t, 2H, J=6.8 Hz, 1 × OCH_2), 3.11 (m, 1H, 1 × CH–O), 2.34–0.67 (m, 86H, 6 × CH, 31 × CH_2, 6 × CH_3). MS (FAB^+): m/z calculated for $C_{60}H_{100}O_4$, 884.76; found, 884.73. Elemental analysis: calculated for $C_{60}H_{100}O_4$, C 81.39, H 11.38; found, C 81.33, H 11.49%.

2.2.15. Cholsteryloxypentyl 3-(4-(*n*-octadecyloxy)phenyl)-acrylate (ChO5CO18). R_f=0.72 in 15% EtOAc–hexanes; yield: 64%. IR (KBr pellet): ν_{max} in cm^{-1} 2923, 2851, 1701, 1604, 1252, 1174. UV–visible: λ_{max}=310.51 nm, $\in = 2.92 \times 10^4\,L\,mol^{-1}\,cm^{-1}$. ^1H NMR (400 MHz, $CDCl_3$): δ 7.65 (d, J=16 Hz, 1H, 1 × olefinic), 7.47 (d, J=8.2 Hz, 2H, Ar), 6.8 (d, J=8.6 Hz, 2H, Ar), 6.32 (d, J=16 Hz, 1H, 1 × olefinic), 5.34 (brd, J=4.8 Hz, 1H, 1 × olefinic), 4.19 (t, 2H, J=6.5 Hz, 1 × OCH_2), 3.99 (t, 2H, J=6.6 Hz, 1 × OCH_2), 3.49 (t, 2H, J=6.5 Hz,

$1 \times OCH_2$), 3.12 (m, 1H, $1 \times$ CH–O), 2.4–0.67 (m, 84H, $6 \times CH$, $30 \times CH_2$, $6 \times CH_3$). MS (FAB^+): m/z calculated for $C_{59}H_{99}O_4Na$ (M+1), 894.75; found, 894.45. Elemental analysis: calculated for $C_{59}H_{98}O_4$, C 81.32, H 11.34; found, C 81.10, H 11.80%.

2.2.16. Cholsteryloxyhexyl 3-(4-(*n*-octadecyloxy)phenyl)-acrylate (ChO6CO18). R_f=0.72 in 15% EtOAc–hexanes; yield: 63%. IR (KBr pellet): ν_{max} in cm^{-1} 2918, 2849, 1698, 1626, 1249, 1177. UV–visible: λ_{max}=310.71 nm, $\in = 4.43 \times 10^4\,L\,mol^{-1}\,cm^{-1}$. ^1H NMR (400 MHz, $CDCl_3$): δ 7.64 (d, J=15.9 Hz, 1H, $1 \times$ olefinic), 7.47 (d, J=8.6 Hz, 2H, Ar), 6.89 (d, J=8.6 Hz, 2H, Ar), 6.32 (d, J=15.9 Hz, 1H, $1 \times$ olefinic), 5.32 (brd, J=5.1 Hz, 1H, $1 \times$ olefinic), 4.2 (t, 2H, J=6.5 Hz, $1 \times OCH_2$), 3.99 (t, 2H, J=6.5 Hz, $1 \times OCH_2$), 3.49 (t, 2H, J=6.6 Hz, $1 \times OCH_2$), 3.15 (m, 1H, $1 \times$ CH–O), 2.44–0.67 (m, 86H, $6 \times CH$, $31 \times CH_2$, $6 \times CH_3$). MS (FAB^+): m/z calculated for $C_{60}H_{101}O_4$ (M+1), 885.76; found, 885.40. Elemental analysis: calculated for $C_{60}H_{100}O_4$, C 81.39, H 11.38; found, C 81.49, H 11.60%.

2.2.17. Cholsteryloxyheptyl 3-(4-(*n*-octadecyloxy)phenyl)-acrylate (ChO7CO18). R_f=0.74 in 15% EtOAc–hexanes; yield: 69%. IR (KBr pellet): ν_{max} in cm^{-1} 2924, 2849, 1702, 1632, 1250, 1169. UV–visible: λ_{max}=310.53 nm, $\in = 2.83 \times 10^4\,L\,mol^{-1}\,cm^{-1}$. ^1H NMR (400 MHz, $CDCl_3$): δ 7.64 (d, J=15.9 Hz, 1H, $1 \times$ olefinic), 7.47 (d, J=8.6 Hz, 2H, Ar), 6.89 (d, J=8.7 Hz, 2H, Ar), 6.31 (d, J=16 Hz, 1H, $1 \times$ olefinic), 5.34 (brd, J=4.8 Hz, 1H, $1 \times$ olefinic), 4.19 (t, 2H, J=6.6 Hz, $1 \times OCH_2$), 3.99 (t, 2H, J=6.5 Hz, $1 \times OCH_2$), 3.46 (t, 2H, J=6.8 Hz, $1 \times OCH_2$), 3.12 (m, 1H, $1 \times$ CH–O), 2.43–0.67 (m, 88H, $6 \times CH$, $32 \times CH_2$, $6 \times CH_3$). MS (FAB^+): m/z calculated for $C_{61}H_{102}O_4$, 921.78; found, 921.00. Elemental analysis: calculated for $C_{61}H_{102}O_4$, C 81.45, H 11.43; found, C 81.46, H 11.85%.

2.2.18. Cholsteryloxyoctyl 3-(4-(*n*-octadecyloxy)phenyl)-acrylate (ChO8CO18). R_f=0.74 in 15% EtOAc–hexanes; yield: 70%. IR (KBr pellet): ν_{max} in cm^{-1} 2920, 2850, 1702, 1604, 1257, 1166. UV–visible: λ_{max}=310.50 nm, $\in = 1.76 \times 10^4\,L\,mol^{-1}\,cm^{-1}$. ^1H NMR (400 MHz, $CDCl_3$): δ 7.64 (d, J=15.9 Hz, 1H, $1 \times$ olefinic), 7.47 (d, J=8.6 Hz, 2H, Ar), 6.89 (d, J=8.7 Hz, 2H, Ar), 6.32 (d, J=15.9 Hz, 1H, $1 \times$ olefinic), 5.35 (brd, J=5.0 Hz, 1H, $1 \times$ olefinic), 4.20 (t, 2H, J=6.6 Hz, $1 \times OCH_2$), 3.99 (t, 2H, J=6.5 Hz, $1 \times OCH_2$), 3.46 (t, 2H, J=6.8 Hz, $1 \times OCH_2$), 3.12 (m, 1H, $1 \times$ CH–O), 2.36–0.67 (m, 90H, $6 \times CH$, $33 \times CH_2$, $6 \times CH_3$). MS (FAB^+): m/z calculated for $C_{62}H_{104}O_4$, 912.79; found, 912.90. Elemental analysis: calculated for $C_{62}H_{104}O_4$, C 81.52, H 11.48; found, C 81.75, H 11.84%.

2.2.19. Cholsteryloxypentyl 3-(4-(*n*-docosyloxy)phenyl)-acrylate (ChO5CO22). R_f=0.78 in 15% EtOAc–hexanes; yield: 66%. IR (KBr pellet): ν_{max} in cm^{-1} 2919, 2849, 1704, 1604, 1252, 1171. UV–visible: λ_{max}=310.57 nm, $\in = 2.47 \times 10^4\,L\,mol^{-1}\,cm^{-1}$. ^1H NMR (400 MHz, $CDCl_3$): δ 7.65 (d, J=15.9 Hz, 1H, $1 \times$ olefinic), 7.47 (d, J=8.6 Hz, 2H, Ar), 6.89 (d, J=8.7 Hz, 2H, Ar), 6.31 (d, J=15.9 Hz, 1H, $1 \times$ olefinic), 5.34 (brd, J=5.0 Hz, 1H, $1 \times$ olefinic), 4.19 (t, 2H, J=6.6 Hz, $1 \times OCH_2$), 3.99 (t, 2H, J=6.5 Hz, $1 \times OCH_2$), 3.49 (t, 2H, J=6.5 Hz, $1 \times OCH_2$), 3.13 (m, 1H, $1 \times$ CH–O), 2.37–0.67 (m, 92H, $6 \times CH$, $34 \times CH_2$, $6 \times CH_3$). MS (FAB^+): m/z calculated for $C_{63}H_{107}O_4Na$ (M+1), 750.81; found, 751.40. Elemental analysis: calculated for $C_{63}H_{106}O_4$, C 81.58, H 11.52; found, C 81.52, H 11.82%.

2.2.20. Cholsteryloxyhexyl 3-(4-(*n*-docosyloxy)phenyl)-acrylate (ChO6CO22). R_f=0.79 in 15% EtOAc–hexanes; yield: 64%. IR (KBr pellet): ν_{max} in cm^{-1} 2919, 2850, 1699, 1604, 1249, 1178. UV–visible: λ_{max}=310.82 nm, $\in = 2.97 \times 10^4\,L\,mol^{-1}\,cm^{-1}$. ^1H NMR (400 MHz, $CDCl_3$): δ 7.64 (d, J=15.9 Hz, 1H, $1 \times$ olefinic), 7.47 (d, J=8.7 Hz, 2H, Ar), 6.89 (d, J=8.7 Hz, 2H, Ar), 6.31 (d, J=15.9 Hz, 1H, $1 \times$ olefinic), 5.33 (brd, J=5.0 Hz, 1H, $1 \times$ olefinic), 4.20 (t, 2H, J=6.6 Hz, $1 \times OCH_2$), 3.99 (t, 2H, J=6.5 Hz, $1 \times OCH_2$), 3.47 (t, 2H, J=6.5 Hz, $1 \times OCH_2$), 3.12 (m, 1H, $1 \times$ CH–O), 2.37–0.67 (m, 94H, $6 \times CH$, $35 \times CH_2$, $6 \times CH_3$). MS (FAB^+): m/z calculated for $C_{64}H_{108}O_4$, 940.82; found, 940.05. Elemental analysis: calculated for $C_{64}H_{108}O_4$, C 81.64, H 11.56; found, C 81.74, H 11.86%.

2.2.21. Cholsteryloxyheptyl 3-(4-(*n*-docosyloxy)phenyl)-acrylate (ChO7CO22). R_f=0.82 in 15% EtOAc–hexanes; yield: 65%. IR (KBr pellet): ν_{max} in cm^{-1} 2919, 2849, 1701, 1604, 1249, 1179. UV–visible: λ_{max}=310.30 nm, $\in = 2.75 \times 10^4\,L\,mol^{-1}\,cm^{-1}$. ^1H NMR (400 MHz, $CDCl_3$): δ 7.64 (d, J=15.9 Hz, 1H, $1 \times$ olefinic), 7.47 (d, J=8.6 Hz, 2H, Ar), 6.89 (d, J=8.7 Hz, 2H, Ar), 6.31 (d, J=15.9 Hz, 1H, $1 \times$ olefinic), 5.34 (brd, J=4.9 Hz, 1H, $1 \times$ olefinic), 4.19 (t, 2H, J=6.6 Hz, $1 \times OCH_2$), 3.99 (t, 2H, J=6.6 Hz, $1 \times OCH_2$), 3.46 (t, 2H, J=6.8 Hz, $1 \times OCH_2$), 3.12 (m, 1H, $1 \times$ CH–O), 2.37–0.67 (m, 96H, $6 \times CH$, $36 \times CH_2$, $6 \times CH_3$). MS (FAB^+): m/z calculated for $C_{65}H_{110}O_4$, 954.84; found, 954.01. Elemental analysis: calculated for $C_{65}H_{110}O_4$, C 81.70, H 11.60; found, C 81.63, H 11.63%.

2.2.22. Cholsteryloxyoctyl 3-(4-(*n*-docosyloxy)phenyl)-acrylate (ChO8CO22). R_f=0.83 in 15% EtOAc–hexanes; yield: 69%. IR (KBr pellet): ν_{max} in cm^{-1} 2919, 2849, 1699, 1605, 1249, 1175. UV–visible:

λ_{max}=310.60 nm, $\in$=3.07×10^4 L mol^{-1} cm^{-1}. ^{1}H NMR (400 MHz, $CDCl_3$): δ 7.65 (d, J=15.9 Hz, 1H, 1 × olefinic), 7.47 (d, J=8.6 Hz, 2H, Ar), 6.89 (d, J=8.7 Hz, 2H, Ar), 6.32 (d, J=15.9 Hz, 1H, 1 × olefinic), 5.34 (brd, J=5.0 Hz, 1H, 1 × olefinic), 4.19 (t, 2H, J=6.6 Hz, 1 × OCH_2), 3.99 (t, 2H, J=6.5 Hz, 1 × OCH_2), 3.46 (t, 2H, J=6.8 Hz, 1 × OCH_2), 3.13 (m, 1H, 1 × CH–O), 2.34–0.67 (m, 98H, 6 × CH, 37 × CH_2, 6 × CH_3). MS (FAB^+): m/z calculated for $C_{66}H_{113}O_4$ (M+1), 969.86; found, 969.70. Elemental analysis: calculated for $C_{66}H_{112}O_4$, C 81.76, H 12.07; found, C 81.46, H 11.84%.

3. Results and discussion

3.1. *Evaluation of thermal behaviour*

All the new dimers as well as some of the intermediates, i.e. **1a**–**1d** and **2d**, were probed for their phase behaviour with the help of POM and DSC measurements. To the best of our knowledge, the well-known intermediates, **1a**–**1d**, have not been investigated for their LC behaviour hitherto. Thus, they were investigated in this respect; the results are summarized in table 1.

As can be seen, they displayed an enantiotropic SmA phase and/or chiral nematic (N*) phase; one of the material stabilized a short-lived twist grain boundary (TGB) phase, additionally. All the systems showed a strong tendency to have large homeotropic domains on untreated glass slides. The presence of the N* phase was evidenced by the observation of a focal-conic texture, which on mechanical shearing furnishes a Grandjean planar texture. On cooling further, the planar texture of the N* phase changes to a focal-conic fan coexistent with a pseudo-isotropic texture, which is the typical of the SmA phase. The existence of the SmA was further evidenced based on the observation of characteristic focal-conic texture (figure 1 a) in slides treated for planar orientation and a dark field of view for slides treated for homeotropic orientation. The TGB phase showed the filament texture (figure 1 b) on heating from a homeotropic SmA phase. That is, for compound **1d** having a very narrow temperature range of TGB, N* and SmA phases coexisted along with TGB, which was apparent from the fact that the textural patterns pertaining to these three phases appeared concurrently for a short while. The well-known 4-*n*-alkoxycinnamic acids **2a**–**2c** exhibited both nematic (N) and smectic C (SmC) phases in a manner reminiscent of other reports [16]. However, the hitherto unknown 4-*n*-docosyloxycinnamic acid **2d** displayed the SmC phase solely. The N phase was identified by its marble texture (figure 1 c) that flashed when sheared. The occurrence of SmC phase was identified based on the observation of a broken focal conic texture in slides treated for homogenous alignment and the schlieren texture (figure 1 d) (with 4-brush defects) in substrates treated for homeotropic surface conditions. However, both focal conic and schlieren textures were seen when examined in untreated glass plates.

Table 1. Phase transition temperatures (°C)[a] and enthalpies [J g^{-1}] of the intermediates **1a**–**1d** and **2d**. (SmA=smetic A phase; N*=chiral nematic phase; TGB=twist grain boundary phase).

Compound	Heating Cooling
1a	Cr 58.4 [10.9] SmA 101.7 [5.4] I I 100.9 [5.1] SmA[d]
1b	Cr 72.5 [27.5] SmA 92.9 [1.1] N* 97.2 [0.4] I I 96.4 [0.3] N* 91.9 [1] SmA 46.6 [14.3] Cr
1c	Cr 75.9 [33.6] SmA 90.7 [1.2] N* 97.2 [1.1] I I 96.4 [1] N* 89.4 [1.1] SmA 47 [30.6] Cr
1d	Cr 66.8 [28.5] SmA 77.1 [0.5] TGB[b,c]−N* 89.1 [0.8] I I 87.8 [0.7] N*−TGB[b,c] 75.4 [0.5] SmA 45.3 [24.8] Cr
2d	Cr 121.4 [70.4] SmC 150.2 [14.3] I I 146.7 [15.8] SmC 117.8 [67.6] Cr

[a]Peak temperatures in the DSC thermograms obtained during the first heating and cooling cycles at 5°C/min. [b]TGB is a transient phase and it can have either SmA or SmC blocks. [c]The phase transition was observed under polarizing microscope and was too weak to be seen in DSC. [d]DSC scans show that the SmA phase supercools to − 55°C (the lowest temperature that can be attained by the instrument).

The transition temperatures and the associated enthalpies obtained for the dimers **ChO*n*CO*m*** are shown in table 2. These dimers are discrete, since they possess smaller mesogenic unit, the cinnamoate moiety. Importantly, as shown in figure 2 a, in dimers with odd-parity (pentamethylene and heptamethylene) spacer, both the anisometric segments lie almost parallel each other to give an overall rod-like shape in their all-*trans* conformation; as mentioned earlier, this can be ascribed to the acrylate group that connects 4-*n*-alkoxybenzene segment and cholesteryl entity via an alkylene spacer. Owing to this structural feature, they behave categorically different from their analogous dimers comprising even-parity spacer.

From the table 2, it can be seen that the dimers with odd number of methylene units show higher clearing temperatures. The melting temperatures of even-parity members are lower than those of odd ones. Figure 3 illustrates the effect of the number of methylene units (n) in the spacer on the transition temperatures. The investigations revealed that all the odd-parity members of the dimers, i.e. **ChO5CO*m*** and **ChO7CO*m*** (m=12, 16, 18, 22) exhibit the N* phase with or without TGBC* phase, with the exception of one of the dimers

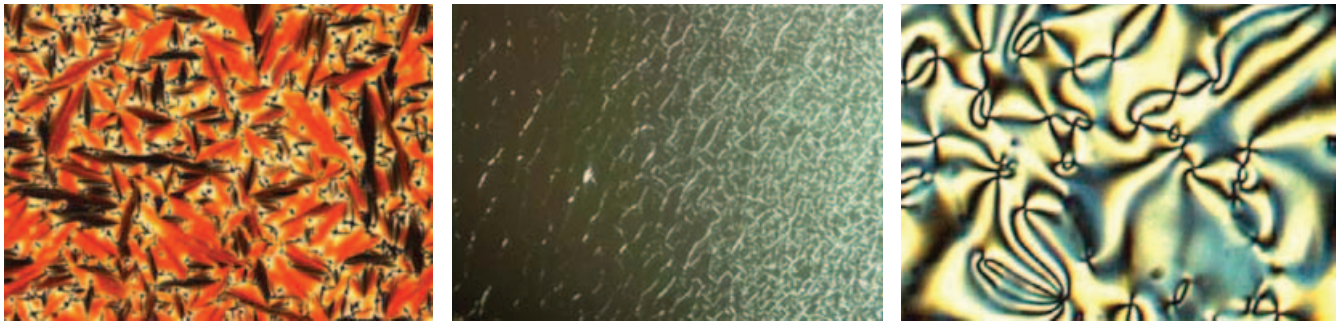

(*a*) (*b*) (*c*)

Figure 1. Microphotographs of the textures of different mesophases: (a) SmA phase (90°C) of **1a**; (b) TGB phase of **1d**; (c) SmC phase (140°C) of **2d**.

(**ChO5CO22**) for which two TGB phases were observed. In particular, the dimers **ChO5CO12** and **ChO7CO12** stabilize an enantiotropic N* phase that was adjudged based on the textural observations.

When a thin film of the sample prepared between two untreated glass slides and cooled from the isotropic phase, the focal-conic texture was obtained, which on mechanical stressing yielded an oily streak pattern

Table 2. Phase transition temperatures (°C)[a] and enthalpies [J g^{-1}] of the **ChO*n*CO*m*** series. (M and M_1 are unknown phases; TGBC*=twist grain boundary phase having chiral smectic C (SmC*) blocks; TGB=twist grain boundary phase with either SmA or SmC blocks).

Compound	Heating Cooling
ChO5CO12	Cr 93.6 [65.5] N* 107.3 [4.4] I I 103.9 [4.1] N* 39.1 [52.8] Cr
ChO6CO12	Cr 60.2 [36.5] I I 35.7 [26.2] Cr
ChO7CO12	Cr 78.2 [46.8] N* 97 [5.6] I I 96.3 [5.4] N* 49.3 [32.7] Cr
ChO8CO12	Cr 61 [71.2] M 65.2 [0.6] I I 65 [0.6] M 49.1 [0.3] M_1 39.6 [29.8] Cr
ChO5CO16	Cr 86 [52.5] N* 101.6 [5.3] I I 101 [5.1] N* 77.4 TGBC*[b] 45 [45.2] Cr
ChO6CO16	Cr 56.3 [25.5] I I 38.1 [19.8] Cr
ChO7CO16	Cr 79.1 [31.1] N* 92.9 [5.5] I I 92.2 [5.2] N* 72.2 [0.6] TGBC* 57.9 [25.3] Cr
ChO8CO16	Cr 56.3 [42.3] I I 44.5 [33.8] Cr
ChO5CO18	Cr 79.9 [59.9] TGBC*[b] 89.6 N* 100 [6] I I 99.4 [6.8] N* 88.5 TGBC*[b] 38.9 [29] Cr
ChO6CO18	Cr 59.6 [58.5] I I 58.8 [1] N* 55.1 [0.6] TGB 51.5 [0.4] TGBC* 42.7 [41] Cr
ChO7CO18	Cr 71.1 [37.4] TGBC* 78.1 [0.4] N* 90.6 [6.9] I I 89.7 [6.9] N* 77.7 [0.4] TGBC* 45.8 [27.2] Cr
ChO8CO18	Cr 52.7 [47.3] TGB[b] 55.1 N* 61.9 [0.9] I I 61.2 [0.8] N* 53.2 [0.3] TGB 51.6 [0.4] TGBC* 41.3 [36.8] Cr
ChO5CO22	Cr 65.7 [35.8] TGBC*[b] 87.8 TGB 93.2 [10.6] I I 92.1 [8.7] TGB 86.1 TGBC*[b] 52.5 [35.6] Cr
ChO6CO22	Cr 71.2 [79.2] I I 59.6 [6.6] N* 53.8 [58.6] Cr
ChO7CO22	Cr 72.2 [56.7] TGBC* 84.2 [0.4] N* 89.4 [12.4] I I 88.1 [11.1] N* 83.3 [0.3] TGBC* 52.7 [37.2] Cr
ChO8CO22	Cr 60.4 [6.3] Cr_1 63.3 [37] I I 63 [1.5] N* 61.2 [2.1] TGB 58.6 [1.5] TGBC* 55.3 [8.4] Cr

[a]Peak temperatures in the DSC thermograms obtained during the first heating and cooling cycles at 5°C min^{-1}. [b]The phase transtion observed with a microscope was too weak to be detected by DSC.

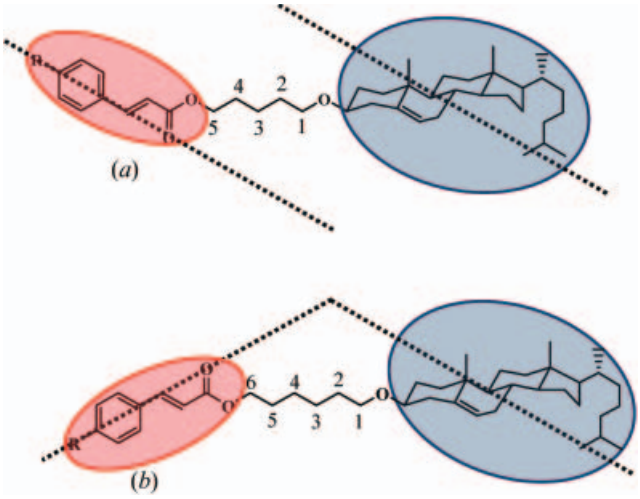

Figure 2. Schematic representation of the molecular shape of non-symmetric dimers possessing an odd number (a) and an even number (b) of alkylene spacers. Notice that in dimers with odd-parity spacer (a) the mesogenic groups are unusually antiparallel

(figure 4 a), which is the typical textural pattern of the N* phase. On increasing the length of the terminal tail, these compounds display TGB phase behaviour, additionally. For example, the dimers **ChO5CO16** and **ChO7CO16** stabilize enantiotropic N* phase and a metastable TGBC* phase, whereas the latter phase also becomes enantiotropic in dimers **ChO5CO18**, **ChO7CO18** and **ChO7CO22**.

It is well known that the structure TGBC* is more complicated than any other TGB phases [17]. Several structures are possible for the TGBC* phase due to the local SmC* tilt of the constituent molecules. However, the occurrence of the square grid pattern for planar boundary condition seems to be excellent support for

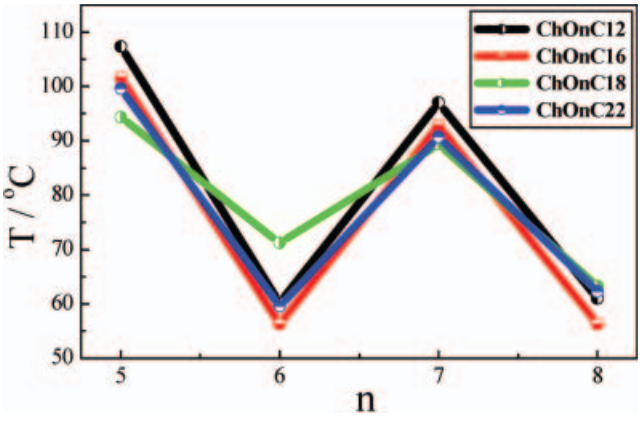

Figure 3. Dependence of the clearing/melting temperatures (T) of dimers on the number of methylene units (n) in the alkylene spacer.

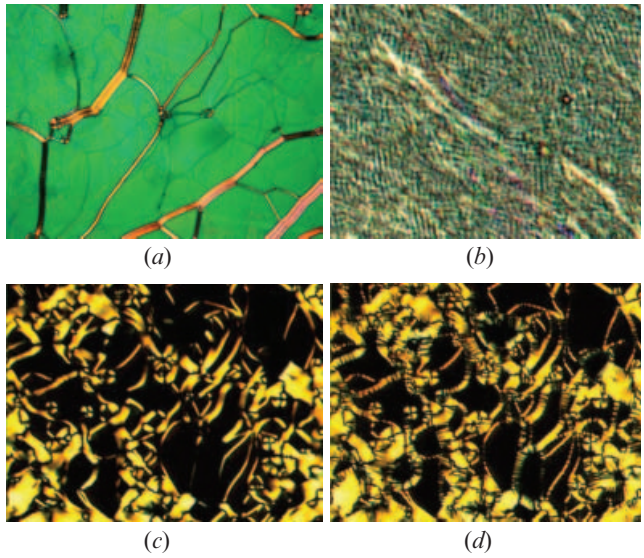

Figure 4. Photomicrographs of the textures of mesophases: (a) N* phase (58°C) of **ChO7CO12**, (b) TGBC* phase (60.5°C) of **ChO7CO16** (c) TGB phase (92°C) and (d) TGBC* phase (80°C) of **ChO7CO22**.

the TGBC* structure proposed by Renn [17b]. In this model, in addition to the intrinsic helical superstructure due to the TGB helix, the SmC* blocks exhibit the director helix of the bulk SmC* phase, with the helix axis perpendicular to that of the TGB helix. In another model referred to as undulated TGBC* (UTGBC*) phase owing to the undulated nature of the smectic layers, has been proposed [17c]. Indeed, experimentally it has been found that the TGBC* or UTGBC* phase displays a striking square grid pattern superimposed on the planar texture as expected. Recently, Clark *et al.* have demonstrated that these features arise from a common structure: ''giant'' smectic blocks of planar layers terminated by grain boundaries [17d]. Thus, on cooling the dimers from the planar pattern of N* phase, the TGBC* phase displayed the characteristic square grid texture, as shown in figure 4 b. On the other hand, when examined on slides treated for homeotropic anchoring conditions and cooled from focal conic texture of N* phase, transition to TGBC* phase occurs wherein the prominent bands appear over the cone-like domains.

As mentioned earlier, for the dimer **ChO5CO22** the exclusive occurrence of the TGB phases, i.e. TGB and TGBC*, was evidenced. This is remarkable given the fact that such behaviour has only recently been disclosed, and thus, restricted to very limited number of optically active LCs [12b]. The sample placed between untreated glass slides and cooled from isotropic liquid, exhibits TGB phase at 92°C having different textural features arising due to both homogeneous

(planar) and homeotropic alignment of the molecules. At first, the TGB grows as droplets that coalesce to a pattern consisting of both the Grandjean planar and the blurred pseudo-focal conic fan texture. Indeed, around the air packets and at the edges of slide, striking filaments were found to occur predominantly (figure 4 c) which is, in fact, considered to be the conclusive evidence for the presence of TGB phase [12b, 17]. When a thin sample was examined in slides treated for either planar or homeotropic anchoring condition, planar pattern or filament texture was seen, as expected. On cooling further, the TGB phase transforms into TGBC* phase at which the filaments of the TGB phase get undulated sharply, as shown in figure 4 d. When examined on slides treated for planar anchoring conditions and cooled from planar texture of TGB phase, transition to TGBC* phase occurs with square grid pattern. Thus, dimers **ChO5CO22** exhibits an interesting liquid crystal phase sequence, i.e. I–TGB–TGBC*, in which two frustrated fluid structures occur over wide temperature ranges.

On the other hand, dimers having even-parity spacer and either *n*-dodecyloxy or *n*-hexadecyloxy tail were found to be crystalline, with the exception of one of the dimers, i.e. **ChO8CO12**, for which two mesophases were adjudged. The optical textures of these two mesophases of **ChO8CO12** were non-specific, which we describe as follows. On cooling the isotropic liquid a mesophase (hereafter refer to as M) appears with pseudo-isotropic texture that on mechanical shearing yields a low birefringent pattern, as shown in figure 5 a. On further cooling the M phase to a temperature of 49°C, another mesophase (M_2) appears with a birefringent non-specific texture, which on shearing furnishes a pattern having some oily streaks like structures (figure 5 b). Identical texture patterns were observed for these two mesophases when slides treated for either planar or homeotropic orientations were used. In contrast, all the higher homologues comprising *n*-octadecyloxy and *n*-docosanyloxy tails exhibited mesomorphism. Specifically, the dimers **ChO6CO18**, **ChO8CO18** and **ChO8CO22** exhibited the N*, TGB and TGBC* phases. These phases were found to be monotropic in the case of dimers **ChO6CO18** and **ChO8CO22**, whereas only the TGBC* was noted to be metastable for **ChO8CO22**. A supercooled metastable N* phase was observed for dimer **ChO6CO22**. In general, it can be seen that these systems do not favour the formation of layered (smectic) structures, implying that these molecules prefer the parallel organization among themselves without any microphase segregation of incompatible regions.

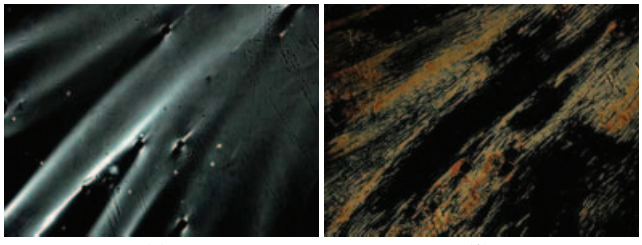

(*a*) (*b*)

Figure 5. Microphotographs of textures of mesophases (sheared) of **ChO8CO12**: (a) M at 53°C; (b) M_1 at 47°C.

3.2. *Optical properties of chiral nematic phase*

The Grandjean (planar) texture of the N* phase exhibits two important optical phenomena namely, the selective reflection and extremely large optical activity [1, 2]. If the pitch length of the N* phase is of the order of the wavelength of incident white light, then colours are selectively reflected. In general, the selective reflection wavelength depends on the molecular chirality and ordering of the molecules within the phase. Importantly, the helical pitch is temperature dependent and thus, the colour of the reflected light varies with temperature, a feature that has been well used in temperature-sensing devices. In recent times, cholesterol-based dimers have proven to be promising in modulating the selective reflection wavelength of the N* phase by changing the parity of the spacer. For example, recent investigations on such dimers have shown that the selective reflection wavelength of the N* phase displays an odd–even effect as a function of the parity of the interlinking spacer. Thus, selective reflection property of the N* phase formed by the **ChO*n*CO*m*** series of dimers was examined with the help of UV–visible–NIR scanning spectrophotometer equipped with a programmable hot stage. The dimer under investigation, in its isotropic phase, was filled in a quartz cell and cooled slowly. When the N* phase is formed, it was subjected to mechanical stress to obtain planar texture in which the helix of the phase becomes normal to the glass plates and the phase reflects incident light. Figure 6 shows the dependence of the selective reflection wavelength (measured from the transmission spectra) on the temperature of N* phase obtained during cooling cycles. It may be mentioned that for dimers **ChO6CO18** and **ChO6CO22** the measurement could not be performed as they stabilized the N* phase over a short-thermal range. In general, the N* phase of the dimers with odd-parity (pentamethylene and heptamethylene) spacer are expected to selectively reflect the light of higher wavelengths when compared to that of even-parity members [18]. However, for these dimers, the odd–even effect is not really convincing; instead, the

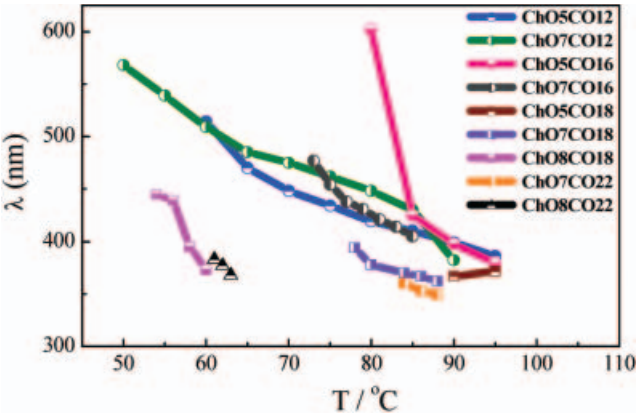

Figure 6. Selective reflection wavelengths of the N* phase of dimers **ChO*n*CO*m*** as a function of temperature.

length of the terminal alkoxy tail seems to be effective. For example, the members with medium alkoxy tail ($OC_{12}H_{25}$ and $OC_{16}H_{33}$) lengths have selective reflection wavelength that is higher than those with longer tails ($OC_{18}H_{37}$ and $OC_{22}H_{45}$). Overall, it can be seen that the absorption maximum (λ_{max}) shifts to longer wavelengths (red shift occurs) as the temperature is lowered. Thus, the thermal dependence of λ_{max} in the entire range of the N* phase of some dimers demonstrates a strong variation in the pitch as the temperature is varied, which is one of the important parameters necessary for practical application.

As a representative case, the N* phase of dimer **ChO5CO12** was subjected to the chiroptical measurement as a function of temperature with the aid of circular dichroism (CD). It may be recalled here that due to helical structure, the N* phase exhibits CD phenomenon wherein the incident light gets resolved into its two circularly polarized components, left and right, at a given wavelength. At this wavelength, depending upon the helical sense (chirality) of the phase, circularly polarized light of a particular handedness is completely reflected while its counterpart is transmitted. Thus, the selective reflection of circularly polarized light of one sense at chiral nematic pitch band should nearly correspond to the one obtained in the UV–visible spectrum. The thin film of the dimer prepared during the selective reflection measurement by UV–visible spectroscopic method was used for this study. As shown in figure 7 a, for all the scans a very strong, wide and positive CD band, besides two weak peaks, were observed. The λ_{max} values and intensities of the CD signals are listed in table 3. The λ_{max} of the strong CD bands are on the lower side when compared to the values obtained in selective reflection, as summarized in table 3. For comparison, the absorption spectrum recorded for the same dimer is shown in

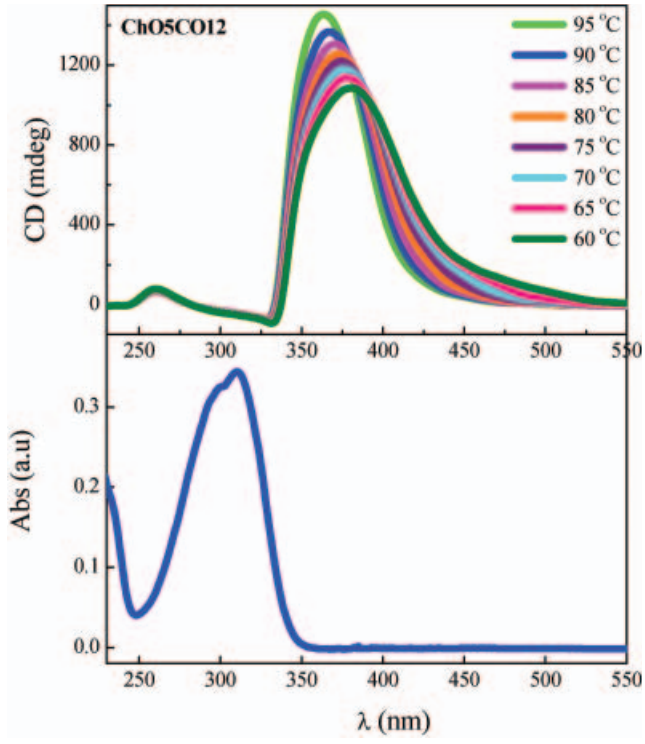

Figure 7. (a) The temperature dependence of the CD spectra of the N* phase recorded in the cooling cycle for dimer **ChO5CO12**. (b) UV–visible spectrum in solution (CH_2Cl_2) obtained for dimer **ChO5CO12**.

figure 7 b. In general, it can be seen that the intensity of the CD band increases monotonically on lowering the temperature with a slight bathochromic shift. Thus, chiroptical study formally evidence the helical structure of the N* phase wherein intermolecular interactions between electronic transitions occur. Importantly, the positive sign of the CD band, as per convention, indicates a right-handed screw sense of the chiral nematic structure which is in accordance with the fact that most steroidal esters are right-handed.

3.3. *Electrochemical properties*

Studying the electrochemical behaviour of LC dimers appears to be essential to validate their multifunctional characteristics. Cyclic voltammetry (CV) is the most widely and frequently used technique for acquiring the information about electrochemical properties of a given system. Thus, as a representative case, the oxidation and reduction potentials of dimer **ChO5CO12** were measured by CV [19]. A conventional three-electrode cell, consisting of 1mm diameter platinum disc as a working electrode, silver–silver chloride as a reference electrode and the platinum wire as a counter electrode, were used. The reference electrode consisted of a silver wire

Table 3. Temperature dependant UV–visible and CD data obtained for the N* phase of dimer **ChO5CO12**.

Temperature/°C	UV–vis λ_{max}/nm	CD λ_{max}/nm	CD CD signal/mdeg
95	386	363, 327, 260	+1457, −72, +67
90	399	366, 332, 260	+1368, −70, +64
85	410	370, 329, 260	+1307, −71, +64
80	419	372, 330, 260	+1258, −75, +67
75	434	374, 329, 260	+1224, −78, +70
70	448	375, 329, 259	+1186, −84, +73
65	470	377, 330, 260	+1141, −88, +75
60	514	380, 331, 260	+1087, −91, +78

suspended in the electrolyte solution saturated with lithium chloride. The electrochemical potential of silver was calibrated with respect to ferrocene/ferrocenium (Fc/Fc+) couple. Tetrabutylammonium hexafluorophosphate (0.1M) in dichloromethane was used as a supporting electrolyte (buffer). The redox potentials of dimer **ChO5CO12** (10^{-3}M in buffer) was measured at a scanning rate of 0.05 V s^{-1}; the cyclic voltammogram (figure 8 a) shows a reduction wave at $E_{red}=-1.227$ V and an oxidation wave at $E_{ox}=2.112$ V. The electrochemical band gap, ΔE_{CV}, between the frontier orbital LUMO and HOMO was determined from the CV by taking the difference between the onset of oxidation and reduction potential. Of course, to the onset redox potentials 4.7 eV (vs. $Ag/Ag^{+}Cl^{-}$) was added, prior to the ΔE_{CV} determination. The band gap determined (figure 8 b) was found to be 3.3 eV. The band gap (ΔE) was also deduced from the red edge of the longest wavelength absorption, $\lambda_{red\ edge}=356$ nm (figure 7 b), using the expression $E=h\upsilon$ (where $\upsilon=c/\lambda$) and was found to be 3.4 eV [19]. Apparently, ΔE deduced from both the methods are comparable, indicating that these compounds genuinely possess electro-activity.

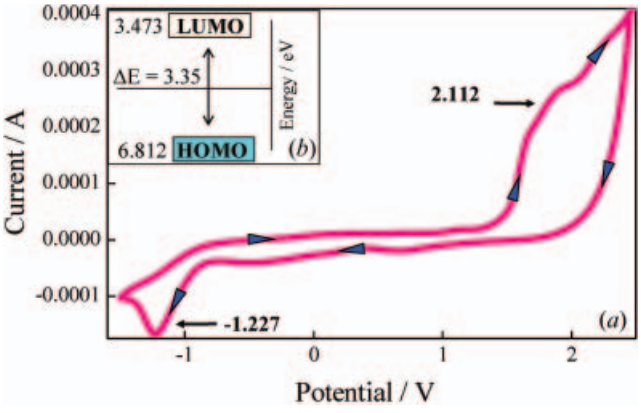

Figure 8. (a) Cyclic voltammogram of dimer **ChO5CO12** in CH_2Cl_2 at scan rate of 0.05 V s^{-1}. (b) Schematic representation of band gap between LUMO and HOMO.

4. Conclusion

We have synthesized and studied the thermal behaviour of an altogether new set of non-symmetrical chiral dimers in which the smaller mesogenic (cinnamoate) core is combined covalently with the cholesteryl segment through a paraffinic spacer. The length and parity of the spacer, as well as the length of the alkoxy tail were varied to understand the structure–property correlation. The key intermediates to target dimers also have been examined for their liquid crystal behaviour. A strong odd–even effect has been observed for the thermal properties of these target dimeric materials. The dimeric compounds comprising odd-parity spacer exhibit chiral nematic and/or twist grain boundary phases. However, the members with even-parity spacer are either crystalline or exhibit metastable chiral nematic and/or twist grain boundary phases. Selective reflection measurements revealed that, for these dimers, the odd–even effect is not persuasive; instead, the length of the terminal alkoxy tail seems to be effective. However, in some cases, the thermal dependence of wavelength of reflected visible light in the entire mesophase range was noted. Cyclic voltammetry experiments revealed the electrochemical property of a liquid crystal dimer. We are continuing our work on different dimers possessing cinnamoate mesogenic cores.

References

[1] (a) S. Chandrasekhar. *Liquid Crystals*, second edn, Cambridge University Press, Cambridge (1992); (b) P.J. Collings, J.S. Patel. *Handbook of Liquid Crystal Research*, Oxford University Press, New York (1997); (c) P.G. de Gennes, J. Prost. *The Physics of Liquid Crystals*, Oxford Science Publication, Oxford (1993).

[2] B. Bahadur. *Liquid Crystals: Applications and Uses*, Vols. 1–3, World Scientific, Singapore (1990).

[3] (a) D. Demus. *Liq. Cryst.*, **5**, 75 (1989); (b) C. Tschierske. *J. Mater. Chem.*, **8**, 1485 (1998); (c) C. Tschierske. *J. Mater. Chem.*, **11**, 2647 (2001); (d) C. Tschierske. *Annu. Rep. Prog. Chem. C*, **97**, 191 (2001); (e) C. Tschierske. *Curr. Opin. Colloid Interface Sci.*, **7**, 69 (2002).

[4] (a) C.T. Imrie. *Structure and Bonding – Liquid Crystal II*, D.M.P. Mingos (Ed.), p. 149, Springer-Verlag (1999) and references cited therein; (b) C.T. Imrie, P.A. Henderson. *Curr. Opin. Colloid Interface Sci.*, **7**, 298 (2002).

[5] (a) N. Tamaoki, M. Moriyama, H. Matsuda. *Angew. Chem. Int. Ed.*, **39**, 509 (2000); (b) N. Tamaoki. *Adv. Mater.*, **13**, 1135 (2001); (c) V. Ajay Mallia, N. Tamaoki. *Chem. Soc. Rev.*, **33**, 76 (2004) and references cited therein.

[6] (a) G.S. Attard, S. Garnett, C.G. Hickman, C.T. Imrie, L. Taylor. *Liq. Cryst.*, **7**, 495 (1990); (b) G.S. Attard, R.W. Date, C.T. Imrie, G.R. Luckhurst, S.J. Roskilly, J.M. Seddon, L. Taylor. *Liq. Cryst.*, **16**, 529 (1994); (c) I.D.

Fletcher, G.R. Luckhurst. *Liq. Cryst*., **18**, 175 (1995); (d) A.E. Blatch, I.D. Fletcher, G.R. Luckhurst. *J. Mater. Chem*., **7**, 17 (1997).

[7] A.E. Blatch, I.D. Fletcher, G.R. Luckhurst. *Liq. Cryst.*, **18**, 801 (1995).

[8] (a) A. Yoshizawa, K. Yamamoto, H. Dewa, I. Nishiyama, J. Yamamoto, H. Yokoyama. *J. Mater.* Chem., **13**, 172 (2003); (b) A. Yoshizawa, M. Kurauchi, Y. Kohama, H. Dewa, K. Yamamoto, I. Nishiyama, T. Yamamoto, J. Yamamoto, H. Yokoyama. *Liq. Cryst*., **33**, 611 (2006).

[9] (a) F. Hardouin, M.F. Achard, J.-I. Jin, J.-W. Shin, Y.K. Yun. *J. Phys., Paris II*, **4**, 627 (1994); (b) F. Hardouin, M.F. Achard, J.-I. Jin, Y.K.Yun. *J. Phys., Paris II*, **5**, 927 (1995); (c) S.-W.Cha, J.-I. Jin, M.F. Achard, F. Hardouin. *Liq. Cryst*., **29**, 755 (2002); (d) J.-W.Lee, Y. Park, J.-I. Jin, M.F. Achard, F. Hardouin. *J. Mater. Chem*., **13**, 1367 (2003); (e) K.-N. Kim, E.-D. Do, Y.-W. Kwon, J.-I. Jin. *Liq. Cryst*., **32**, 229 (2005).

[10] (a) C.V. Yelamaggad, S.A. Nagamani, U.S. Hiremath, G.G. Nair. *Liq. Cryst.*, **28**, 1009 (2001); (b) C.V. Yelamaggad, M. Mathews. *Liq. Cryst*., **30**, 125 (2003) and references cited in these articles.

[11] (a) C.V. Yelamaggad. *Mol. Cryst. liq. Cryst.*, **36**, 149 (1999); (b) C.V. Yelamaggad, S.A. Nagamani, D.S. Shankar Rao, S.K. Prasad, U.S. Hiremath. *Mol. Cryst. liq. Cryst*., **363**, 1 (2001).

[12] (a) D.S. Shankar Rao, S. Krishna Prasad, V.N. Raja, C.V. Yelamaggad, S. Anitha Nagamani. *Phys. Rev. Lett.*, **87**, 085540 (2001); (b) C.V. Yelamaggad, A.S. Achalkumar, N.L. Bonde, A.K. Prajapati. *Chem. Mater*., **18**, 1076 (2006).

[13] (a) A.T.M. Marcelis, A. Koudijs, Z. Karczmarzyk, E.J.R. Sudholter. *Liq.Cryst.*, **30**, 1357 (2003); (b) A.T.M. Marcelis, A. Koudijs, E.J.R. Sudholter. *Mol. Cryst. liq. Cryst*., **411**, 1234 (2004).

[14] S. Bhattacharya, Y. Krishnan-Ghosh. *Langmuir*, **17**, 2067 (2001).

[15] W. Shuting, J. Zhiqin, L. Heting, Y. Li, Z. Daixun. *Molecules*, **6**, 52 (2001).

[16] Y.-S. Kang, H. Kim, W.-C. Zin. *Liq. Cryst.*, **28**, 709 (2001).

[17] (a) H.-S. Kitzerow, C. Bahr. *Chirality in Liquid Crystals*, Springer-Verlag, New York (2001); (b) S.R. Renn. *Phys. Rev. A*, **45**, 953 (1992); (c) P.A. Pramod, R. Pratibha, N.V. Madhusudana. *Curr. Sci*., **73**, 761 (1997); (d) J. Fernsler, L. Hough, R.-F. Shao, J.E. Maclennan, L. Navailles, M. Brunet, N.V. Madhusudana, O. Mondain-Monval, C. Boyer, J. Zasadzinski, J.A. Rego, D.M. Walba, N.A. Clark. *PNAS*, **102**, 14191 (2005).

[18] (a) A.T.M. Marcelis, A. Koudijs, E.J.R. Sudholter. *J. Mater. Chem.*, **6**, 1469 (1996); (b) A.T.M. Marcelis, A. Koudijs, E.J.R. Sudholter. *Liq. Cryst.*, **18**, 843 (1995); (c) V.A. Mallia, N. Tamaoki. *J. Mater. Chem*., **13**, 219 (2003).

[19] (a) H.-Y. Wang, J.-C. Feng, G.-A. Wen, H.-J. Jiang, J.-H. Wan, R. Zhu, C.-M. Wang, W. Wei, W. Huang. *New J. Chem.*, **30**, 667 (2006); (b) S.P. Mishra, K. Krishnamoorthy, R. Sahoo, A. Kumar. *J. Mater*. Chem., **16**, 3297 (2006); (c) T. Sotomura, H. Uemachi, K. Takeyama, K. Naoi, N. Oyama. *Electrochim. Acta*, **37**, 1851 (1992); (d) A.L. Kanibolotsky, R. Berridge, P.J. Skabara, I.F. Perepichka, D.D.C. Bardley, M. Koeberg. *J. Am. chem. Soc*., **126**, 13695 (2004).